CHEMICAL CHARACTERIZATION OF CLAY MINERALS WITH CHEMCAM AT THE MARIMBA DRILL LOCATION, GALE CRATER, MARS. G. David[1], A. Cousin[1], O. Forni[1], P-Y. Meslin[1], E. Dehouck[2], G. Berger[1], N. Mangold[3], W. Rapin[4], O. Gasnault[1], R. C. Wiens[5], S. Maurice[1]; [1]IRAP, Toulouse, France, [2]LGL-TPE, Université de Lyon, France, [3]LPG, Nantes, France, [4]Caltech-GPS, Pasadena, USA, [5]LANL, Los Alamos, USA; [gael.david@irap.omp.eu]

Introduction: Since 2012, the Curiosity rover has been investigating the sedimentary rocks of Gale crater. The study of secondary phases such as clay minerals is important to characterize paleo-environments. Among the payload of the rover, the CheMin X-ray diffraction instrument [1] provides local information on the mineral phases present in the bedrock. In most of the drill samples analyzed, clay minerals represent an important fraction of the total minerals phases (up to ~30 wt.%) [2, 3].

Due to its remote sensing method of acquisition, the ChemCam [4, 5] Laser-Induced Breakdown Spectroscopy instrument provides a statistically significant survey of the chemistry of the rocks. The submillimeter (350-550 µm) diameter of the laser beam enables it to probe fine features such as mineral phases. However, due to their small particle size and their mixture with other detrital phases in Gale's rocks, direct detection of clays by ChemCam is challenging.

The goal of this work is to assess the potential of ChemCam to detect clay minerals in the bedrock and to characterize their chemical composition. To this purpose, we compared the ChemCam chemical data to the mineralogical constraints given by CheMin at the Marimba drill location.

Geological setting: Marimba is located in the Karasburg member of the Murray formation. Major crystalline phases present in the drill sample [2, 3] correspond to clay minerals (28 ± 5 wt.%), andesine (14.0 ± 0.9 wt.%), calcium sulfate (7.0 ± 0.6 wt.%), and hematite (6.4 ± 0.4 wt.%). Sanidine and pyroxene are respectively present at 2.4 ± 0.6 wt.% and 0.7 ± 0.6 wt.%. Amorphous material is present at 40 ± 20 wt.%. Clay diffraction peaks are consistent with the presence of Mg-rich trioctahedral and Fe-rich dioctahedral smectite resembling respectively saponite and nontronite and/or Fe-montmorillonite [2].

Data and methods: The ChemCam dataset used for this study included 6 targets acquired on the same rock slab as the Marimba drill location: Marimba, Cabinda, Marimba_Drill_Hole_1420_ccam, Epukiro, Marimba2_ccam, sol1427_Marimba_presieve_dump.

In these data, we first isolate the ChemCam shot-to-shot data points that are assumed to contain a higher proportion of clay minerals. For this, we used the chemical index of alteration (CIA, [6]) that is useful to study alteration products in open-system weathering, as it occurred in the Murray formation [7]. It is based on the ratio of the immobile element (Al_2O_3) relative to mobile elements (Na_2O, CaO, and K_2O) defined as follows, CIA (in molar proportion) = $Al_2O_3/(Al_2O_3+CaO+Na_2O+K_2O)*100$**.** Data points with a CIA>50 in figure 1 (above the plagioclase-K-feldspar join) are assumed to be mostly composed of clay minerals and plagioclase mixtures since no other Al-rich phases were observed by CheMin. Iron oxides are not taken into account by this method. Consequently, a hematite contribution is still present in our selected data but this method enables us to remove the major contribution from some amorphous phases, Ca-rich pyroxenes, and Ca-sulfates, and increase the relative proportion of smectite minerals.

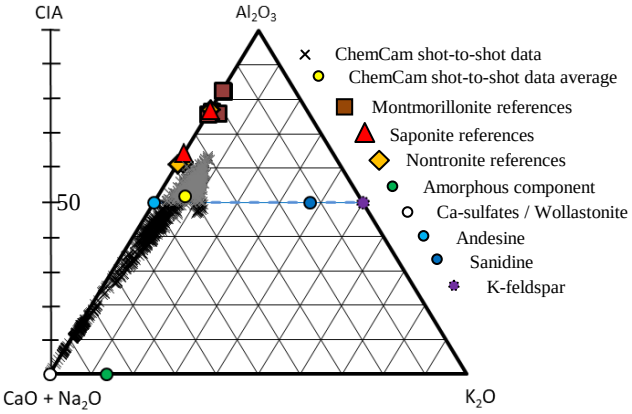

Figure 1: Al_2O_3-CaO+Na_2O-K_2O diagram (in molar proportions) included ChemCam shot-to-shot data (x symbols). ChemCam data with CIA >50 are mostly composed of clay minerals and plagioclase mixtures (grey symbols).

To constrain clay minerals chemistry, we used two ternary diagrams (FeO_T-MgO-Al_2O_3 and SiO_2/4-K_2O+2*CaO+Na_2O-Mg) in order to observe potential trends in the remaining data points. In these diagrams, three natural montmorillonite (Swy-2, SAz-1, STx-1), one Fe-montmorillonite (Braňany), two nontronite (NG-1 and NAu-1) and one saponite (Griffith) compositions are used as references, provided by the Clay Minerals Society and from [8, 9], in addition to the three smectite compositions from MinDat. Major phase compositions such as igneous mineral and the bulk composition of the amorphous component detected by CheMin are also plotted (from [3]).

Results: The FeO_T-MgO-Al_2O_3 ternary diagram (fig. 2) enables to decipher the end-member chemistry of the major smectite minerals (saponite, montmorillonite, and nontronite). The ChemCam dispersion shows three trends toward these different end-members. The trend toward MgO (red x symbols, fig. 2) would correspond mostly to saponite clays or Mg-bearing amorphous

phases, as olivine was not observed at the CheMin limit of detection (~1 wt.%) and pyroxene (possibly enstatite or ferrosilite) was recorded at only 0.7 ± 0.6 wt.% [2].

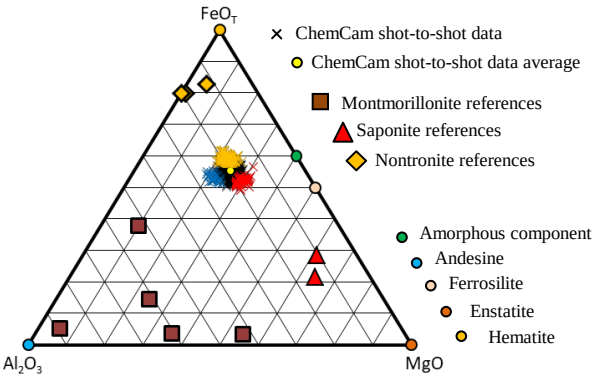

Figure 2: FeO_T-MgO-Al_2O_3 diagram (in molar proportions) included ChemCam shot-to-shot data. Red, blue and orange x symbols correspond respectively to MgO/y>27.5, Al_2O/y>22.5, and FeO_T/y>54, where y= FeO_T+MgO+Al_2O_3

Al-rich points trend toward plagioclase or montmorillonite compositions (blue x symbols, fig. 2). However, the SiO_2/4-(K_2O-2*CaO-Na_2O)-MgO diagram (fig. 3) shows clearly that their compositions are consistent with plagioclase composition rather than montmorillonite.

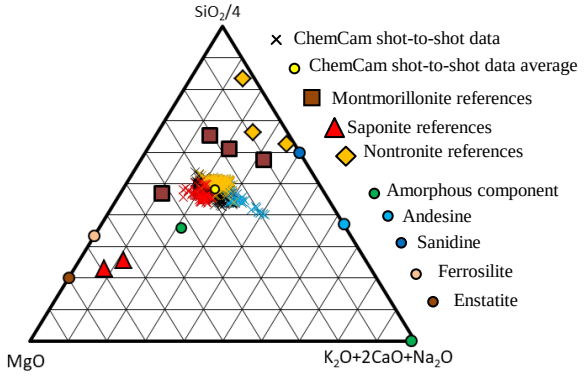

Figure 3: SiO_2/4-(K_2O-2*CaO-Na_2O)-MgO diagram (in molar proportions) included ChemCam shot-to-shot data. Red, blue and orange x symbols correspond respectively to Mg-, Al- and Fe- rich data points identified from figure 2.

Finally, Fe-rich points observed in figure 2 (orange x symbols) trend toward nontronite or iron oxide end-members. However, figure 3 shows that all Fe-rich points are also Si-rich. Contribution from iron oxides would not produce such enrichment in Si. Consequently, Fe-rich points are probably mostly composed of nontronite minerals or amorphous equivalent (i.e., hisingerite that is possibly present within the amorphous component [10]) rather than hematite.

Figure 4 shows the H contents estimated from an independent component analysis [11] as a function of the FeO_T+MgO (from fig. 2). The ICA H scores expressed here correlate with H abundances. The positive correlation observed confirms that Fe- and Mg-rich points are also enriched in H, which is consistent with the presence of clay minerals (nontronite−saponite solid solution) or amorphous phases rather than anhydrous minerals such as pyroxenes or hematite. Conversely, data points enriched in Al (and depleted in FeO_T+MgO) show a weak H signal that is consistent with plagioclase minerals.

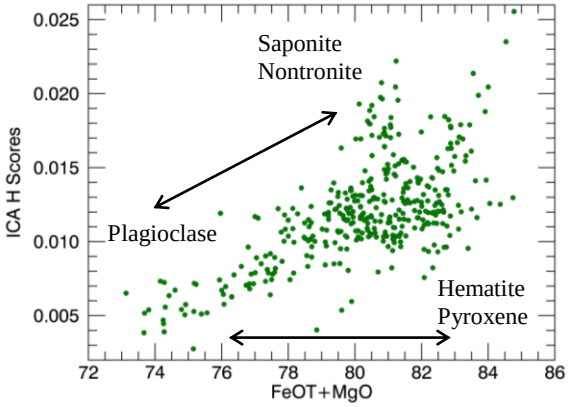

Figure 4: Mg+Fe (defined from figure 2) as a function of the ICA H scores for ChemCam shot-to-shot data points. ChemCam targets composed of powder (drill hole and presieve dump) were removed from the dataset because physical matrix effects can artificially increase the ICA H scores [12].

Conclusion: Our results show that ChemCam is able to observe mixing trends in shot-to-shot data that is potentially related to clay minerals. Two mineral phases with compositions trending toward saponite or/and Mg-rich amorphous material, and nontronite or/and hisingerite are present in the Marimba drill location, whereas (Fe)montmorillonite composition is not visible from our observations.

Future work needs to be done on other Gale crater drill samples to better constrain clay compositions and confirm the good synergy between ChemCam and CheMin. Such work would be particularly useful for the study of the clay-bearing unit (Glen Torridon) that the rover is currently exploring.

References: [1] Blake, D. et al., (2012). *Space Science Reviews*, 170(1), 341-399. [2] Bristow, T. F. et al., (2018). *Sci Adv*, 4(6). [3] Rampe E. B. et al., (submitted). *Chemie der Erde*. [4] Maurice S. et al., (2012), *Space Science Reviews*, 170,95. [5] Wiens R.C. et al., (2012), *Space Science Reviews*, 170, 167. [6] Nesbitt, H. W. et al., (1982). *Nature*, 299, 715-717. [7] Mangold, N. et al., (2019). *Icarus*, 321, 619-631. [8] Novák I. and al., (1978). *Clays and Clay Minerals*, 26, 341-344. [9] Treiman A. H. et al., (2014). *American Mineralogist*, 99, 2234-2250. [10] Dehouck E., et al., (2014). *JGR: Planets*, 119. [11] Forni O. et al., (2013). *Spectrochimica Acta part B*, 86, 31-41. [12] Rapin w. et al., (2017). *Spectrochimica Acta part B*, 137, 13-22.